

## Electronic Supplementary Information

### **Keggin-type polyoxometalate cluster as active component for redox-based nonvolatile memory**

Xiaoli Chen,<sup>a</sup> Pu Huang,<sup>a</sup> Xin Zhu,<sup>b</sup> Suixing Zhuang,<sup>a</sup> Hengcheng Zhu,<sup>a</sup> Jingjing Fu,<sup>b</sup> Arun S. Nissimagoudar,<sup>b</sup> Wu Li,<sup>b</sup> Xiuwen Zhang,<sup>a</sup> Li Zhou,<sup>a</sup> Yan Wang,<sup>a</sup> Ziyu Lv,<sup>a</sup> Ye Zhou <sup>\*b</sup> and Su-Ting Han<sup>\*a</sup>

<sup>a</sup> Shenzhen Key Laboratory of Flexible Memory Materials and Devices, College of Electronic Science and Technology, Shenzhen University, Shenzhen, 518060, P. R. China. E-mail: sutinghan@szu.edu.cn

<sup>b</sup> Institute for Advanced Study, Shenzhen University, Shenzhen, 518060, P. R. China. E-mail: yezhou@szu.edu.cn

## **Experimental section**

*Device fabrication:* Before device fabrication, the glass substrate (2 cm×2 cm) with patterned 80 nm thick of ITO (500 μm width) was cleaned with Decon90, acetone, and deionized water sequentially. Then blended solution of PW and PMMA in Propylene Glycol Monomethyl Ether Acetate (PGMEA) with weight ratio of 1:1 was spin coated onto the pre-cleaned substrate with ITO as bottom electrode to form PW@PMMA film. After annealing of the PW@PMMA film at 120 °C for 30 minutes on a hotplate, 30 nm thick of top electrode (Au, Ag or Al) was deposited by thermal evaporation with a shadow mask (500 μm width) to form 5×5 crossbar patterns, thus render a single device size of 0.25 mm<sup>2</sup>. Furthermore, by using this method, variations of device size deriving from device fabrication processes are ruling out.

*Characterization:* The electrical characterizations of the devices were measured by Keysight B2902A precision source/measure unit in ambient atmosphere. The surface morphology of the as-fabricated PW@PMMA film was characterized by atomic force microscope (AFM, Bruker Dimension Icon, ScanAsyst mode, ScanAsyst-Air). The cross-sectional image of the device was obtained by field-emission gun TEM (FEI Tecnai F20). And the TEM sample was prepared using focus ion beam (Hitachi FB-2100). The EELS analysis was carried out by field-emission TEM (probe-corrected and monochromated FEI Titan) with 300 kV of accelerating voltage using high resolution Gatan imaging filter (GIF Tridiem 865 ER300).

The absorption spectra were measured using an Agilent Cary 60 UV-Visible near infrared spectrophotometer. FT-IR spectrum was measured with Fourier transform Infra-Red spectrometer (Perkin Elmer Spectrum 100). Ultraviolet photoelectron spectroscopy (UPS) and X-ray photoelectron spectroscopy (XPS) measurements were respectively performed on ESCALAB 250XI (Thermo Scientific) with 21.2 eV of He I and 1486.6 eV of Al K $\alpha$  monochromatic source. The Kelvin probe force microscopy (KPFM) real space image was obtained by scanning probe microscopy system by contacting the conductive atomic force microscope tip with the PW film. The tip was biased with consecutively +5 V in an area of 4  $\times$  4  $\mu$ m and -5 V in an area of 1  $\times$  1  $\mu$ m in for charge trapping and extraction operations. Conductive atomic force microscopy (C-AFM) with a conductive cantilever coated with Pt was used to scanning over the surface of the active layer for the purpose of identifying the conductive filaments on both the HRS and LRS with a read voltage of 1.0 V.

*DFT calculations:* The DFT calculations were performed using the projector augmented wave method, as was implemented in the VASP code. The generalized gradient approximation (GGA) with the Perdew–Burke–Ernzerhof exchange-correlation functional was adopted. A plane-wave energy cutoff is set to 550 eV. All the atoms were fully relaxed by the conjugate gradient algorithm until the maximum energy difference and residual forces were less than 10<sup>-5</sup> eV and 0.01 eV/Å. To eliminate the interaction between periodic images of adjacent clusters, the lateral dimensions were chosen to be sufficiently large ( $\sim$ 20 Å). The Heyd–Scuseria–



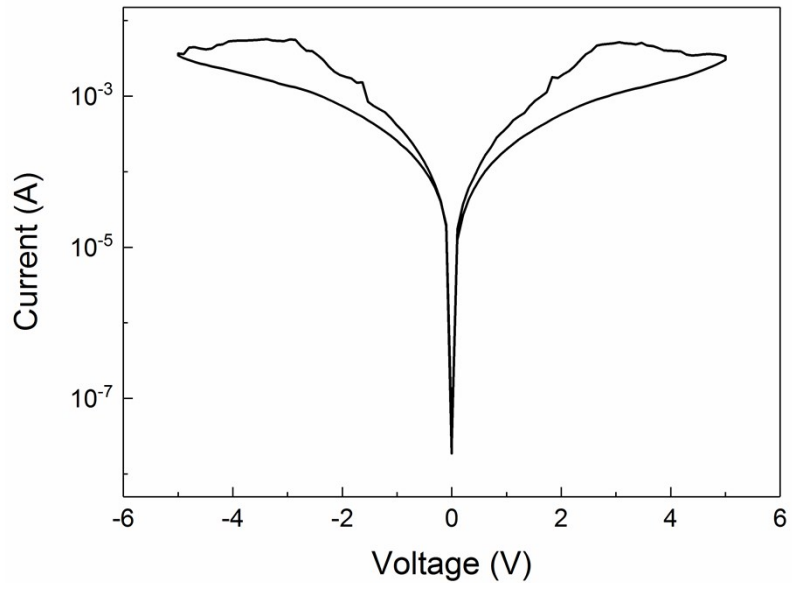


**Fig S2.** I-V characteristics of ITO/ PMMA/Au memory devices

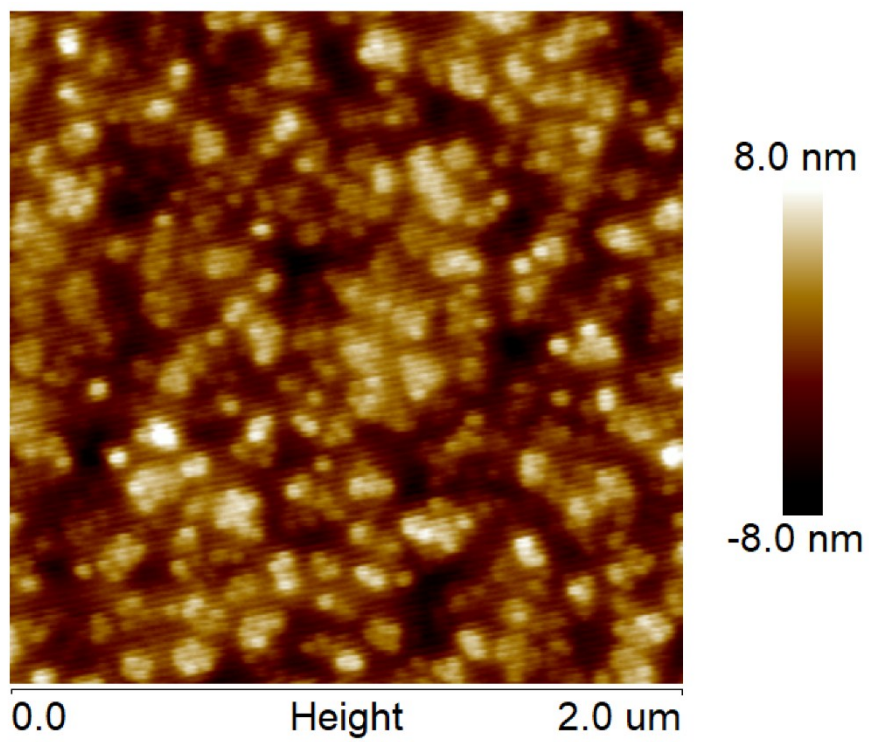


**Fig S3.** The surface morphology of as-fabricated PW@PMMA film

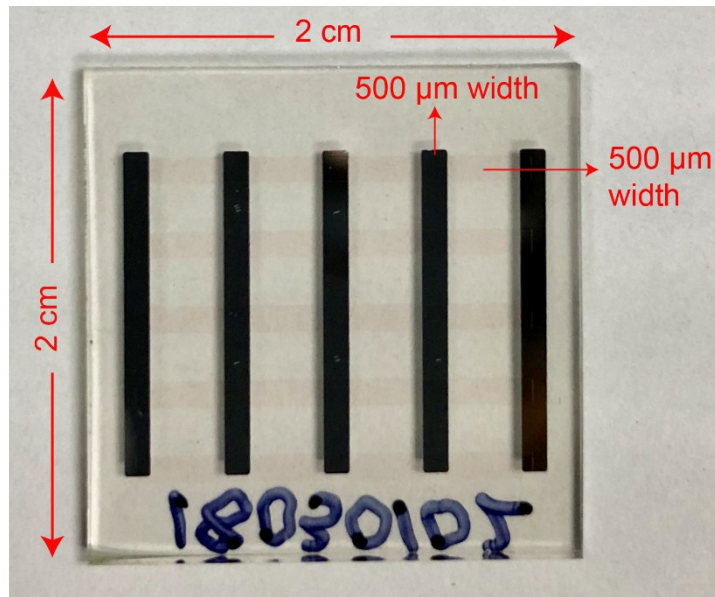


**Fig S4.** The optical image of the as-fabricated memory device

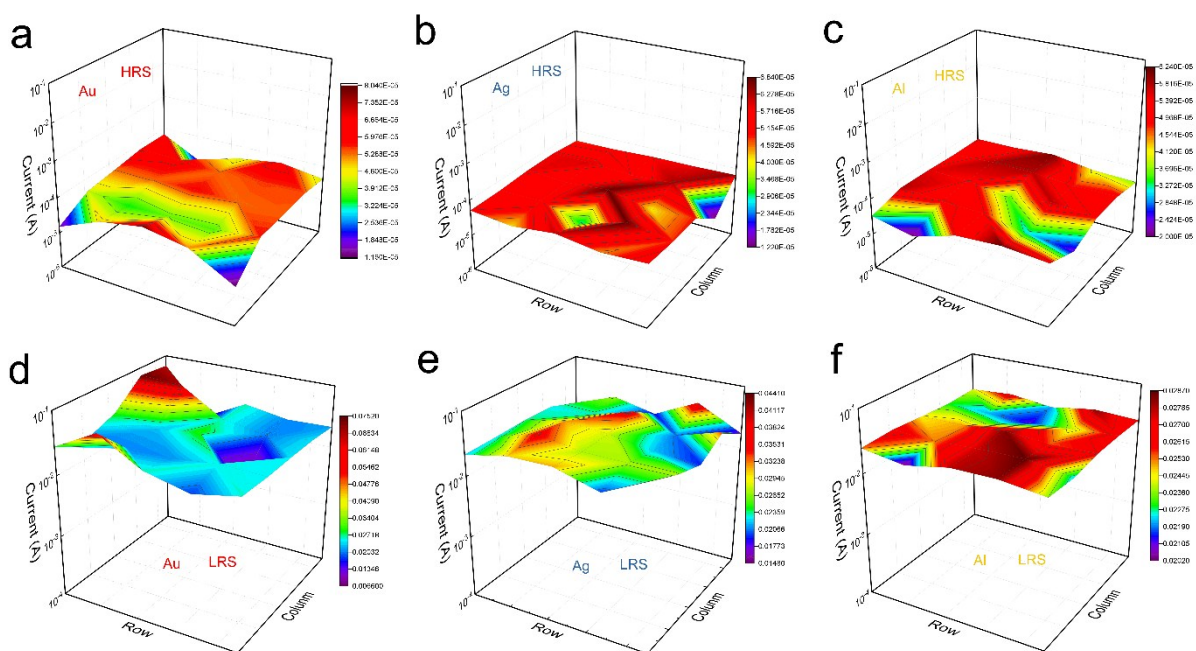


**Fig S5.** Statistical data of current distribution. The current distribution of a) Au; b) Ag; c) Al respectively in their HRS. The current distribution of d) Au; e) Ag; f) Al respectively in their LRS.

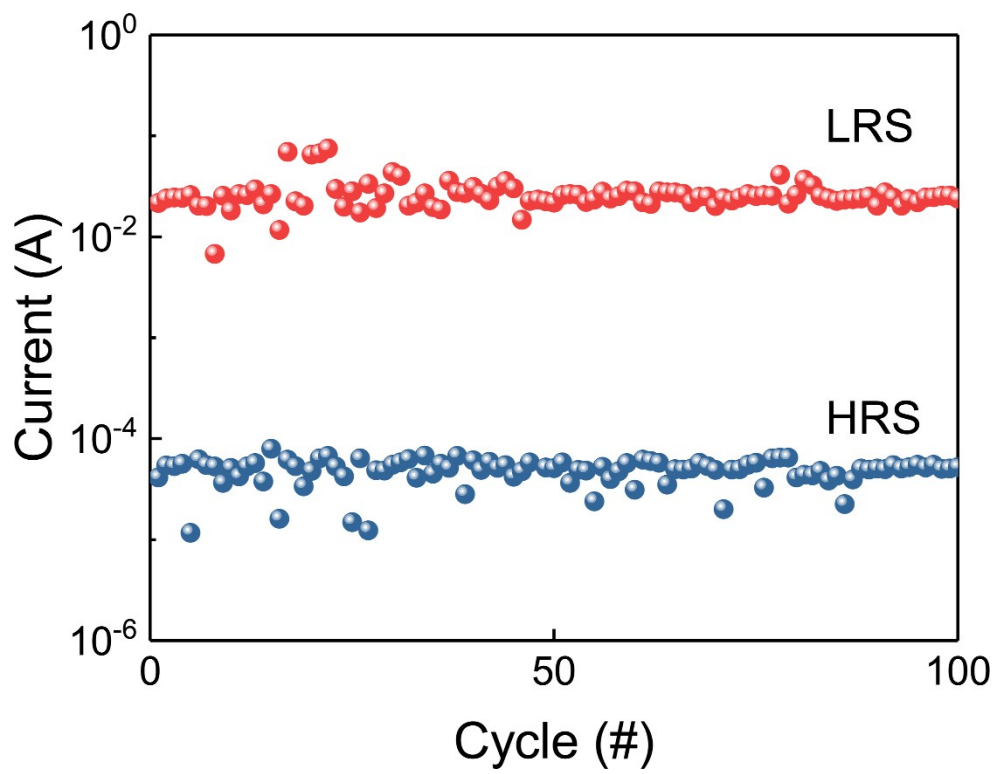


**Fig S6.** The endurance performance of POM-based device in HRS and LRS.

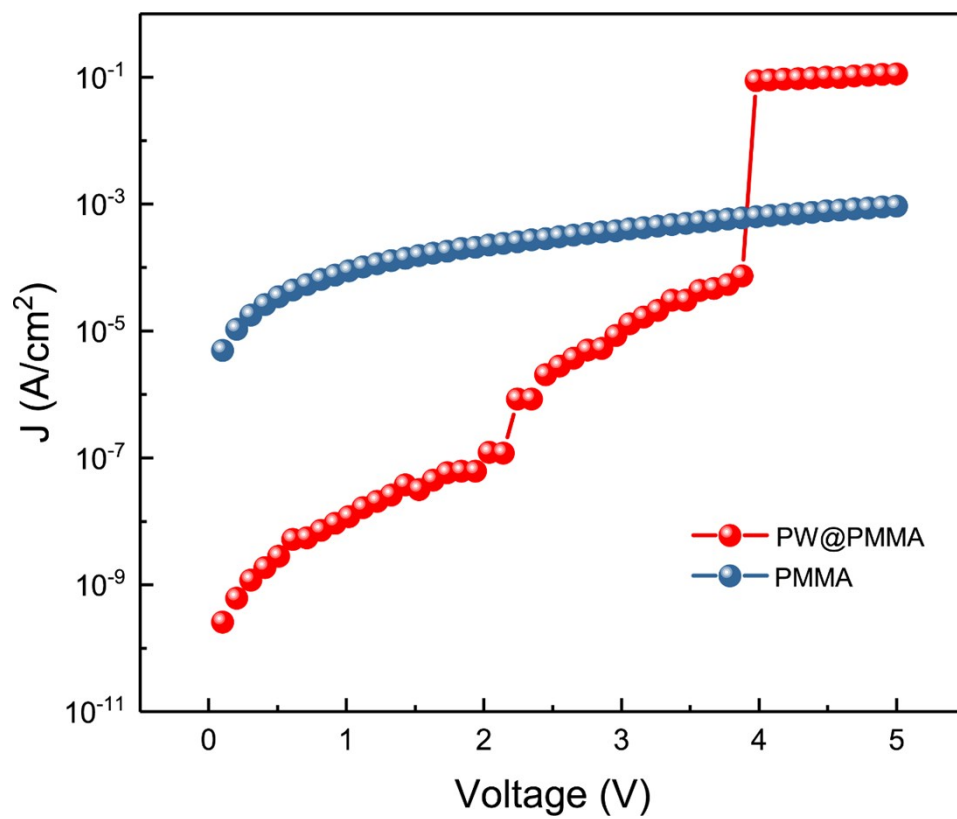


**Fig S7.** J–V characteristics of ITO/PW@PMMA/Au and ITO/ PMMA/Au memory devices.

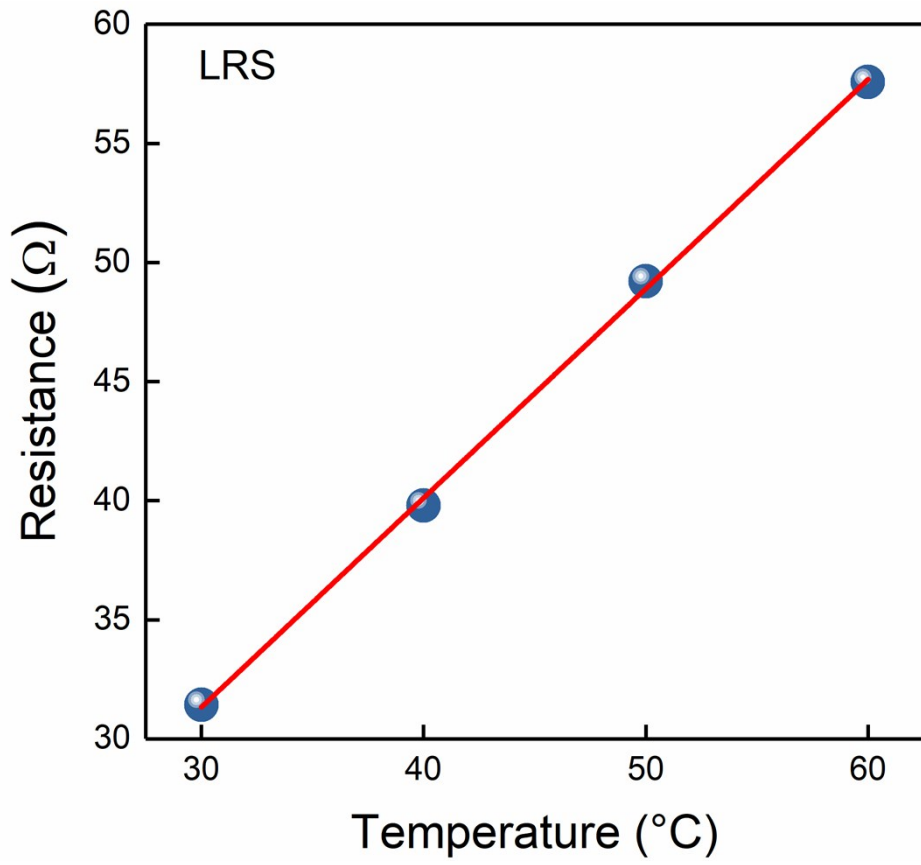


**Fig S8.** The relationship between the resistance of low resistance state and temperature.

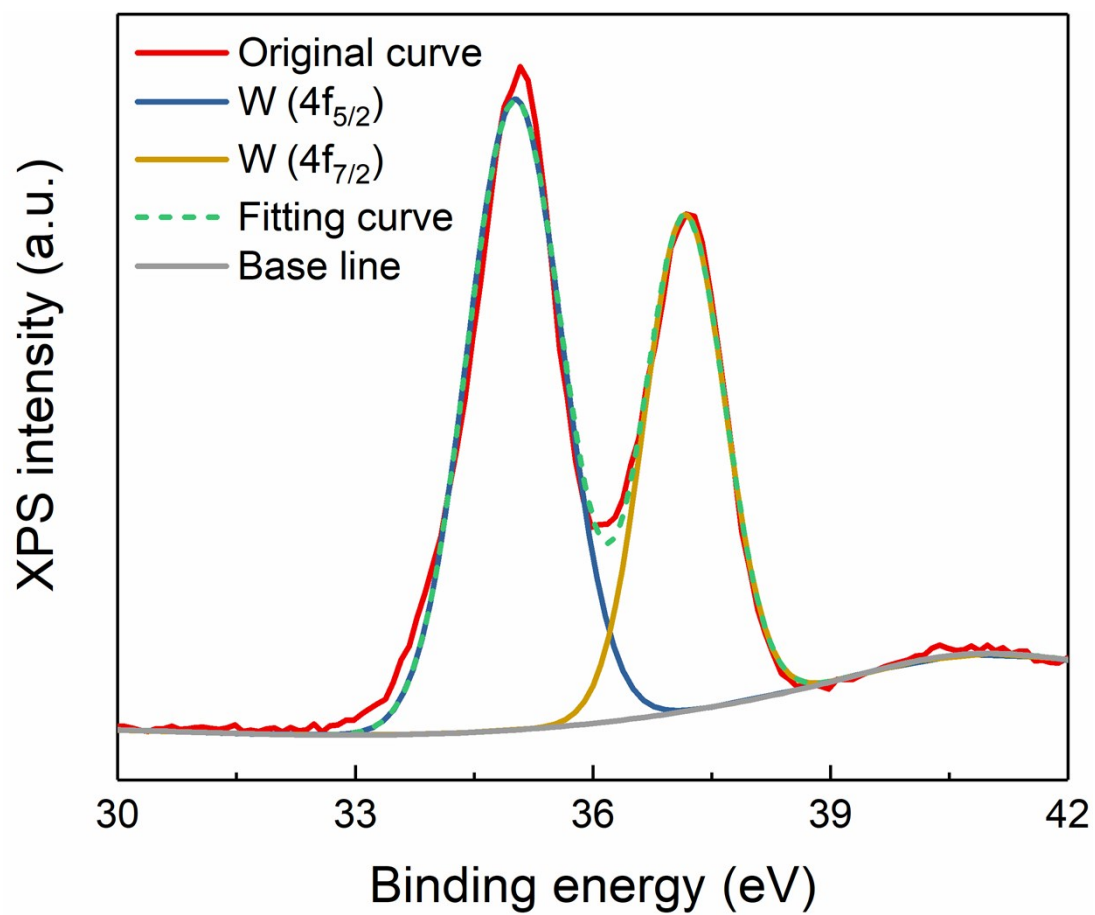


**Fig S9.** W 4f photonemission signal of XPS spectra of the as-fabricated PW film.

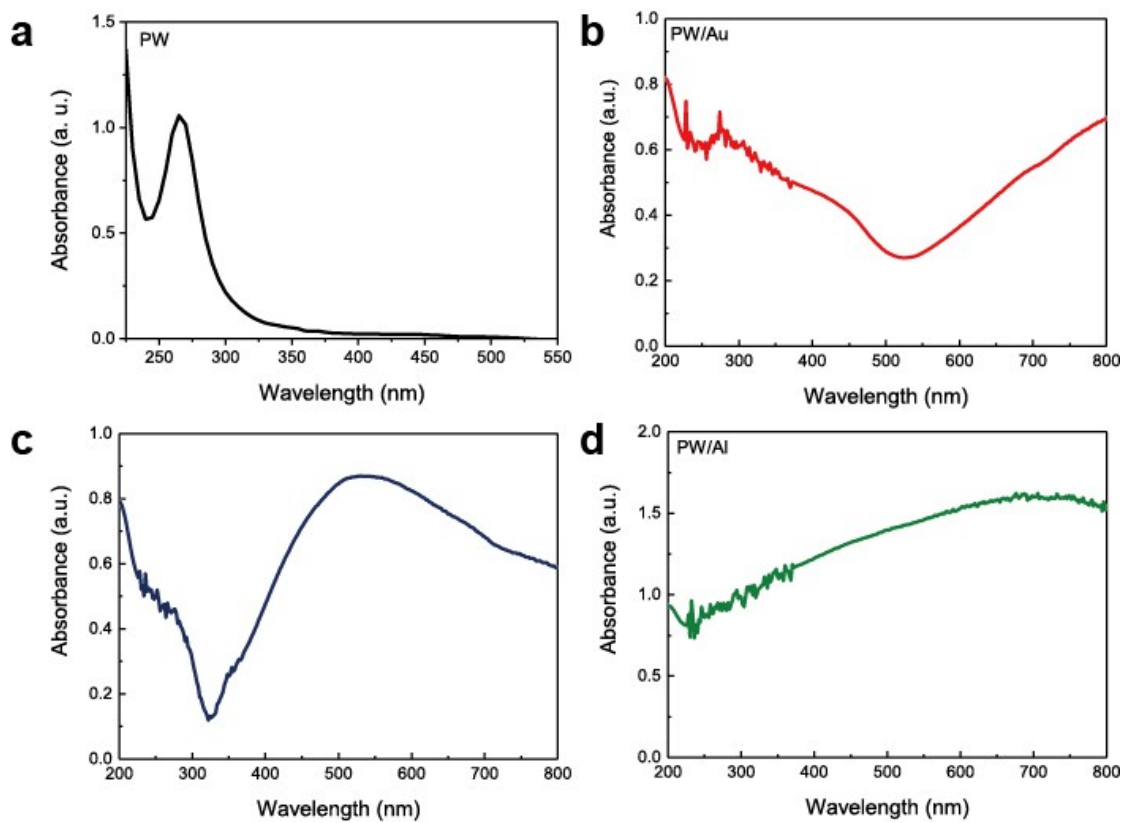


**Fig S10.** UV-vis adsorption of as-fabricated PW film and PW deposited on Au, Ag and Al modified quartz substrate.

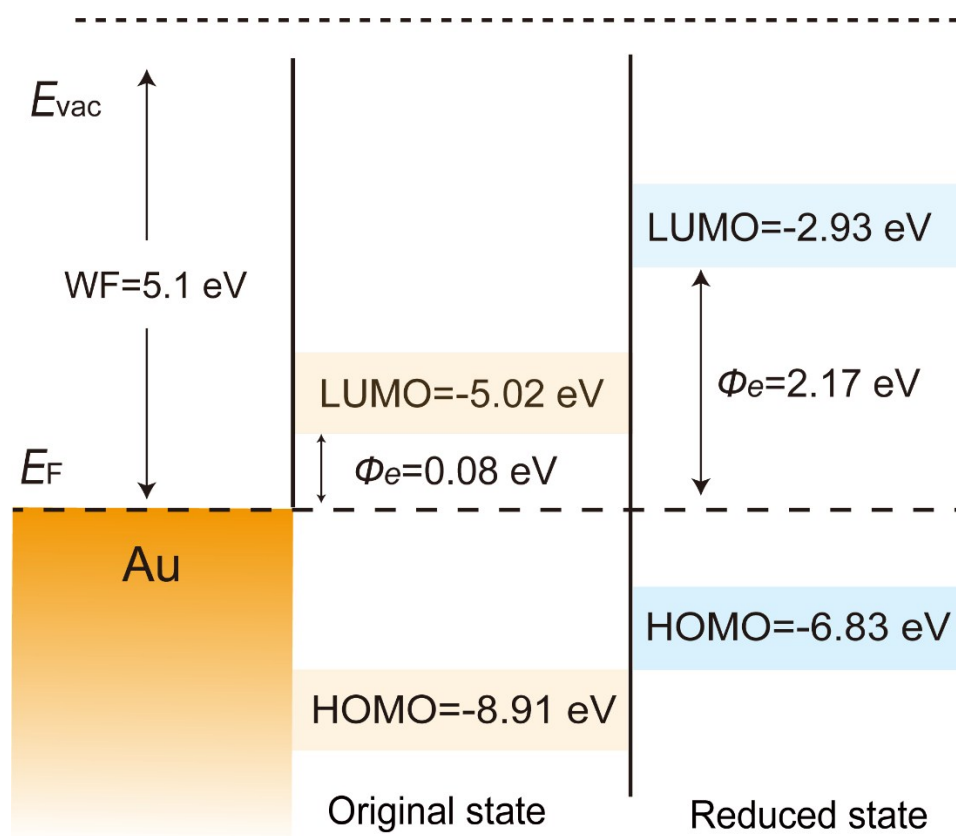


**Fig S11.** The energy level alignment of PW molecule before and after accepting two electrons based on the DFT calculations. The work function value of Au was chosen as 5.1 eV for comparison purpose.

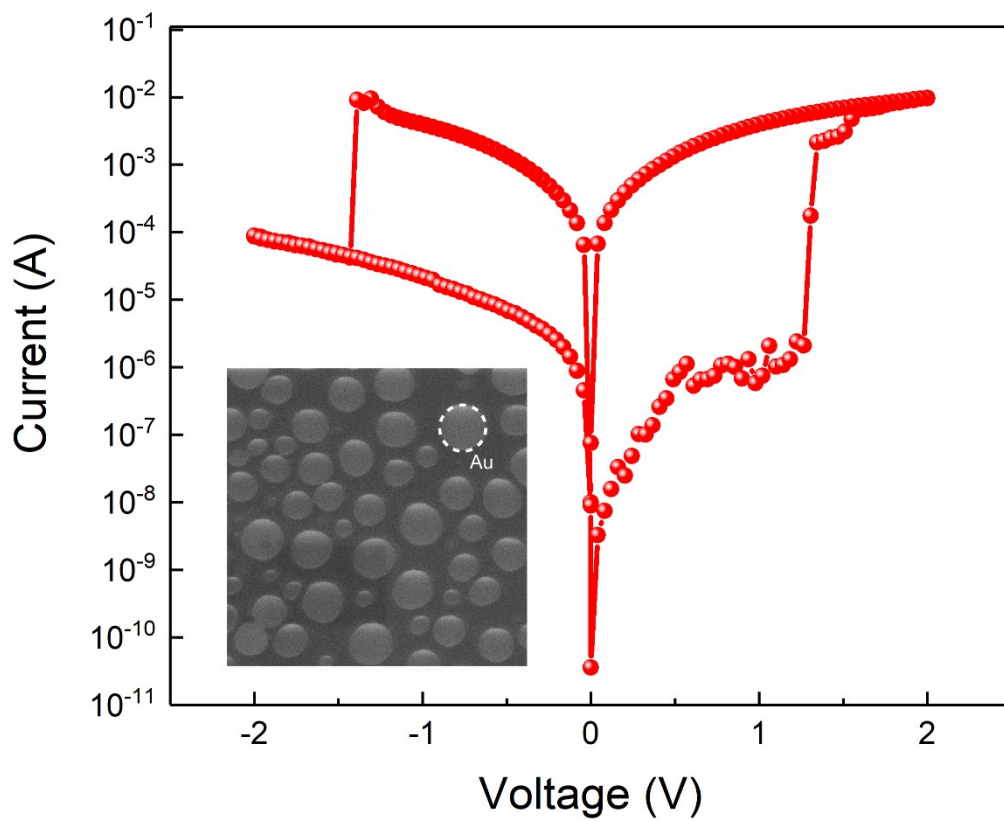


**Fig S12.** The typical I-V characteristic of micrometer PW-based RRAM device. Inset shows the SEM image of the micrometer device with Au as top electrode (cell diameter  $\sim 5 \mu\text{m}$ ).

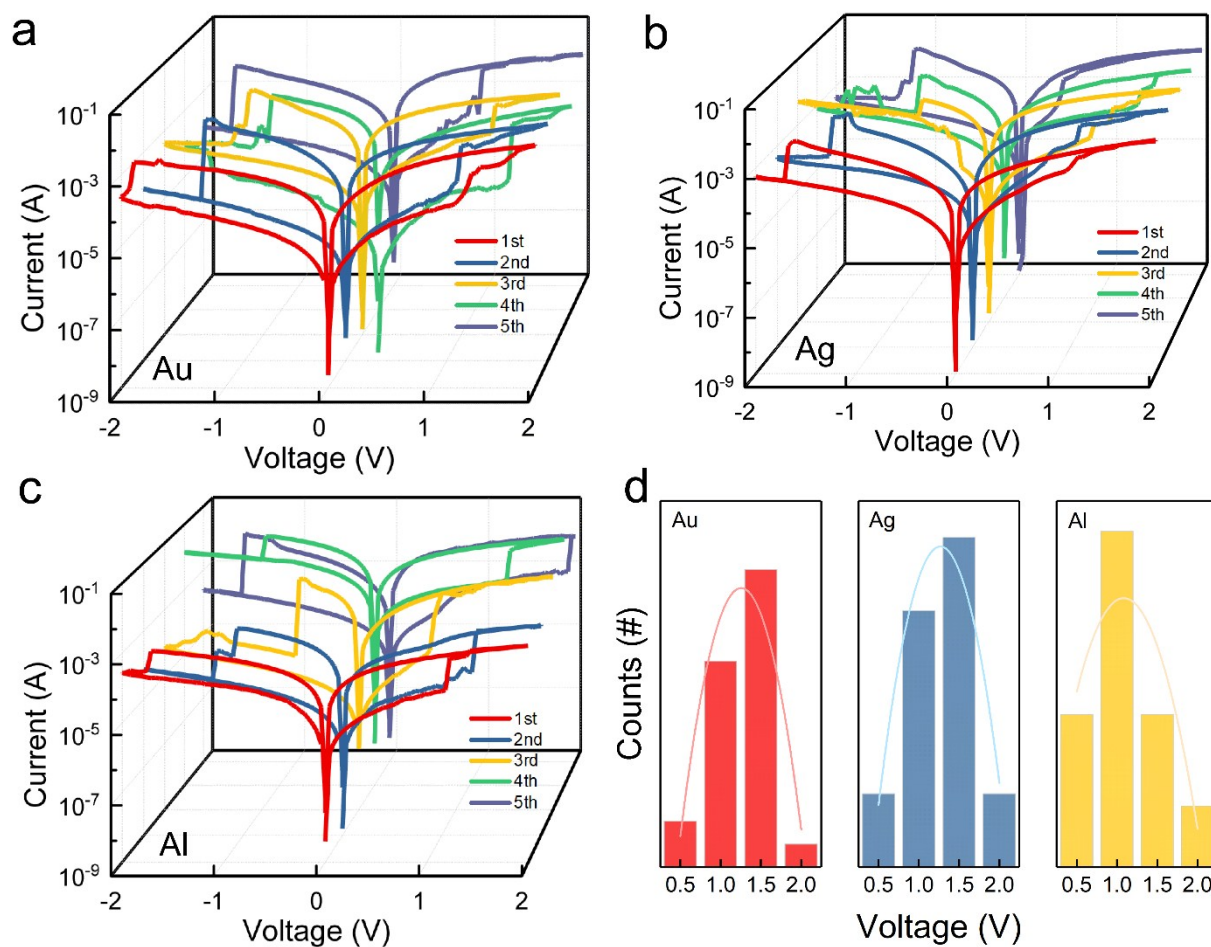


**Fig S13.** Statistical data of Au-, Ag- and Al-based RRAM devices. Five initial typical I-V plot of a) Au; b) Ag; c) Al. d) The distribution of SET voltage with respect to Au-, Ag- and Al-based RRAM devices.